Journal of Chromatography A 1757 (2025) 466145

Contents lists available at ScienceDirect

Journal of Chromatography A

journal homepage: www.elsevier.com/locate/chroma

Gravity stop-flow electrophoresis: A high-power technique for size-based separation of graphene oxide nanosheets

Masoud Shayegan, Hossein Ahmadzadeh *

Department of Chemistry, Faculty of Science, Ferdowsi University of Mashhad, Mashhad, Iran

ARTICLE INFO

Keywords:
Graphene oxide
Size-dependent properties
Nanomaterials separation
Size-based separation
Gravity stop-flow electrophoresis
High-throughput separation

ABSTRACT

Graphene oxide (GO) exhibits size-dependent properties that enable its use in a range of applications. Current techniques for size-based separation of GO face several notable limitations and challenges. The gravity stop-flow electrophoresis (GSFE) technique is introduced here, for the first time, which addresses a large part of the stated limitations. Characterization methods were applied to each collected fractions for further correlation between size of each fraction and their corresponding properties. Characterization experiments including, a) the UV–Vis spectroscopy (Stokes shift from 195.4 nm for the smallest particle to 200.7 nm for the largest particle), b) capillary electrophoresis (migration time changed from 6.8 min for the smallest particle to 5 min for the largest particle), c) zeta potential measurement (changed from 23.3 mV for the largest particle to 37.7 mV for the smallest particle), d) electrophoretic mobility (determined by dynamic light scattering, changed from 2.9 × 10–8 m2V-1s-1 for the smallest particle to 1.8 × 10–8 m2V-1s-1 for the largest particle) and e) transmission electron microscopy for the smallest and the largest particles were performed. Furthermore, the results demonstrated that this technique has a high resolution with less limitations when compared to most classical separation methods. Finally, the most important limitation of capillary electrophoresis was resolved by significantly improving the throughput of separation.

1. Introduction

Nanomaterials (NMs) exhibit distinct chemical, physical, and biological properties that differ from those of bulk materials [1]. As size decreases, the surface-to-volume ratio of NMs increases, resulting in a larger fraction of atoms being exposed on the surface. This alteration significantly impacts their reactivity and physical properties [2,3].

Graphene oxide (GO) is a prominent example of NMs with size-dependent properties that enable its application across various fields. For instance, in membrane separation processes, and the size of graphene oxide (GO) sheets significantly influence enantioseparation efficiency [4]. Additionally, studies have shown that the toxicity and blood compatibility of GO are closely related to factors such as dosage, degree of exfoliation, and sheet dimensions [5]. In the context of electrochemical biosensors, the size of GO sheets plays a critical role in determining the performance of label-free systems, as it can either enhance or hinder the sensitivity of graphene-based electrochemical sensors. Furthermore, precise control over GO sheet size may have substantial implications for optimizing specific biosensing applications [6]. The classification of graphene oxide (GO) nanosheets based on lateral dimensions is not universally standardized and may vary across studies. However, a general categorization include large GO nanosheets with lateral dimensions typically greater than 1000 nm, intermediate GO nanosheets ranging from 100 to 1000 nm, and small GO nanosheets with lateral dimensions <100 nm [7]. Larger GO sheets are often utilized in supercapacitor technology due to their high surface area, which enhances energy storage capabilities through greater electrochemical interactions. For instance, the critical ratio of graphene oxide (GO) to multi-walled carbon nanotubes (W_{GO}/W_{MWCNT}) needed to achieve a stable MWCNT dispersion is directly influenced by the size of the GO sheets. As the GO sheet size decreases from 2060 nm to 170 nm, the minimum W_{GO}/W_{MWCNT} ratio required to fabricate a conductive GO–MWCNT film dropped significantly from 0.1 to 0.025 [8–10].

Intermediate-sized GO finds its application in biomedical fields, such as drug delivery and biosensing, where a balance between surface area and dispersibility is crucial for effective interaction with biological systems. This size allows for functionalization with biomolecules, making it suitable for targeted drug delivery and as a platform for

* Corresponding author.
E-mail address: h.ahmadzadeh@um.ac.ir (H. Ahmadzadeh).

https://doi.org/10.1016/j.chroma.2025.466145
Received 27 February 2025; Received in revised form 1 June 2025; Accepted 11 June 2025
Available online 14 June 2025

Table 1
Comparison of GSFE with Other Methods for the Separation of GO Nanosheets.

Technique	Resolution	Speed	Cost	Preparative Capacity	Main Applications	Throughput	Theory Complexity	Limitations	Advantages	Ref.
Centrifugation	Low to Medium	High	Low	High	Separation of large particles, pre-concentration	Medium	Low	Limited resolution for very small particles	Simplicity, low cost	[25,34,35]
Ultrafiltration	Medium	Medium	High	High	Size-based separation, purification	Low	Low	Membrane fouling, frequent replacement	Suitable for large volumes	[36,37]
Capillary Electrophoresis (CE)	Very High	Low	Medium	Low	High-resolution analysis, charge-based separation	Low for commercial CE	Medium	Very low preparative capacity	High precision	[38–40]
Free-Flow Electrophoresis (FFE)	High	Medium	High	High	High-volume separation of biomolecules	High	High	Requires complex and expensive equipment	High preparative capacity	[41–43]
HPLC	High	Low	High	Medium	Separation of small and medium molecules	Low	High	High cost, expensive columns	Very high precision, versatility	[44,45]
Field-Flow Fractionation (FFF)	High	Medium	High	Medium	Separation of nanoparticles, polymers, biomolecules	High	High	Requires specialized equipment, time-consuming	High precision, no stationary phase required	[27,28,46]
GSFE	High	Medium	Low	Medium	Size- and charge-based separation of nanoparticles	High	Medium	Requires parameter optimization	Simplicity, high precision, low cost	This work

biosensors [2,11,12].

Small-sized GO is particularly effective in environmental applications, such as the adsorption of heavy metal ions and organic pollutants. For instance, ultrasonicated GO demonstrates significant improvements in adsorption capacity due to increased availability of active sites [8,9,13–19].

The versatility of GO is underscored by the critical role that size plays in determining its suitability for various technological advancements. Effective separation of GO nanosheets based on size can enhance the performance of each fraction for specific applications. Classical size-based separation techniques, including centrifugation, membrane filtration, liquid exfoliation, sedimentation, and field-flow fractionation, are employed to achieve desired size distributions [20–23].

However, current techniques for size-based separation of NMs, such as GO, face notable limitations. For example, centrifugation is labor-intensive and time-consuming, often lacking sufficient resolution for particles with small size differences [24,25]. Membrane filtration encounters challenges due to fouling, leading to decreased efficiency and maintenance needs [20,26]. Field-flow fractionation, while advanced, is complex and costly, with limited throughput, hindering scalability for industrial applications [22,26–30]. Some electrophoresis techniques such as single capillary electrophoresis, despite its high resolution, struggles with fraction collection capability. The Free Flow Electrophoresis (FFE) technique, however, overcomes this limitation, as its separation capacity can be enhanced simply by increasing the dimensions of the chamber. Despite several advantages, this method does require specialized equipment, such as a the thermostated flow-through chamber with membrane separated electrode compartments and fraction collector, which may pose a challenge in some settings [31–33]. GSFE has the potential for scale up, and therefore, to overcome the limitation of poor capacity and fraction collection of a single capillary CE instrument. Also the GSFE with the dimensions reported here, has also lower capacity compared to FFE, but has the potential of higher loading capacity if the dimensions of the chamber is scaled up. Particles with different sizes and/or different charges migrate at different rates, allowing for size-based separation. Table 1 provides a comparison between GSFE and other separation techniques for nanomaterials.

To address these challenges, there is an urgent need for improved separation techniques that enhance efficiency, scalability, and precision. This research introduces the gravity stop-flow electrophoresis (GSFE) technique, which aims to resolve many of the stated limitations for size-based separation of material such as macro molecules and NMs. Characterization methods, including UV–Vis spectroscopy, capillary electrophoresis, zeta potential, and transmission electron microscopy, were applied to the collected fractions to correlate their sizes with corresponding properties, validating the separation efficiency of the proposed technique.

2. Methods and materials

2.1. Materials

Only analytical grade reagents were used in this study. Sodium hydroxide (>97 %), silver nitrate (99 %), barium chloride (99 %), hydrochloric acid (37 %), sodium nitrate (99 %) and sodium chloride (99.5 %) from Merck Co (Germany), graphite powder (>95 %) from Fluka, sulfuric acid (95 %) from Riedel, $KMnO_4$ (99 %) from BDH and H_2O_2 (30 %) from Fakhre Razi (Iran) were purchased. Tris(hydroxymethyl) aminomethane (99 %), glycine (gly) (99 %) and dimethyl sulfoxide (DMSO) (99.7 %) were purchased from Aldrich Co (USA). The buffer solutions of tris-gly (pH 10.5) were employed as electrolytes for electrophoresis. Deionized water was prepared (with 0.6 μS conductivity) by a "Hastaran teb, Iran" purification system.

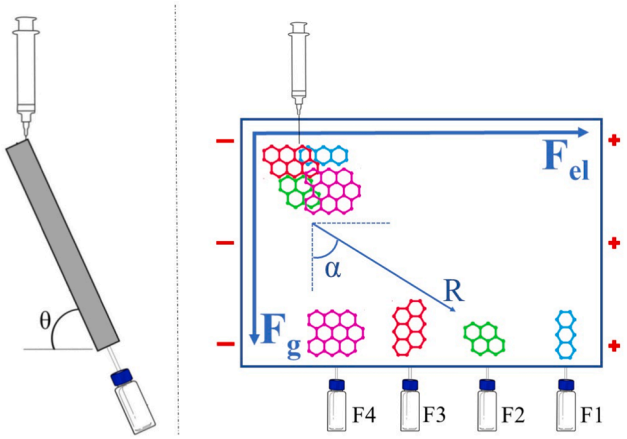

Fig. 1. Experimental setup for gravity stop-flow electrophoresis, the arrows show electrical force F_{el}, gravitational force F_g, the combination of F_{el} and F_g (vectors R), channel angle θ and GO deviation angle α.

2.2. Preparation of GO nanosheets

GO was synthesized using a modified Hummers' method. Briefly, 2 g of graphite powder and 75 ml of concentrated sulfuric acid were mixed in an ice bath. After cooling to 0 °C, sodium nitrate powder (2 g) was gradually added over 15 min while stirring at 300 rpm. Subsequently, potassium permanganate powder (6 g) was slowly introduced into the mixture by continuous stirring in a controlled temperature, resulting in a green color due to the oxidizing agent. Stirring (300 rpm) was continued at room temperature for 2 days. Next, 125 ml of deionized water (DI water) was added, followed by further dilution with water at 32 °C. Finally, hydrogen peroxide (70 ml, 30 %) was added within 40 min. Then, the product underwent centrifugation (10 000 rpm or approximately 11 173 G, 5 min), washing several times with hydrochloric acid (5 wt %), and then deionized water. Classical silver nitrate and barium chloride precipitation tests qualitatively confirmed the removal of Cl^- and SO_4^{2-} ions, respectively. Using a vacuum oven at 60 °C for 48 h, the final product was dried.

2.3. Fabrication of GO in separation channels

The channel was made from plexiglass, which was cut with a laser cutting machine (Fig. 1). The dimensions of channels were 9 × 5.5 cm. The depth of each channel was divided into two parts. The depth of the isolation chamber was 500 μm and that of electrode chamber was 8 mm. This was necessary to have high enough volume of the buffer to prevent the pH change due to the water electrolysis at the electrodes [47]. Two electrodes made of stainless steel with 6 cm long and 300 μm outer diameter (OD) were used to apply voltage on the electrolyte. For electrophoresis the distance between the electrodes was 80 mm. In the lower part of the channel, there were four outlets, which connected the channel to the glass vials through a glass tube with an OD of 1.1 mm and internal diameter, ID, of 1 mm that provided the possibility of fraction collection.

2.4. Size-based separation of GO nanosheets

The separation process was performed in tris-glycine buffer (20 mmol l^{-1} tris and the pH was adjusted to 8.2 by adding glycine to tris). The buffer was degassed in an ultrasonic bath for 10 min. Subsequently, a 5 ml syringe was used to fill the channels and vials with the buffer, and the glass tubes were ventilated prior to each experiment to eliminate the possibility of run-to-run cross contamination.

Six mg of GO nanosheets were dispersed in 2 ml of tris-glycine buffer in an ultrasonic bath at 20 kHz for 30 min. The bulk GO suspension was then injected into the channel with a 1 ml syringe, using a syringe pump at a speed of 200 μl per minute from the top of the channel, near the cathode. Simultaneously with the injection, 130 V was applied to the channel. The separated fractions of the nanosheets were collected in glass vials. For the capillary electrophoresis experiment, a different buffer, tris base-NaCl (tris base 50 mmol l^{-1}, sodium chloride 93 mmol l^{-1}, pH= 10.5), was used and the glass vials were filled with the same buffer.

In the channel of GSFE, it was essential to maintain a static (non-flowing) buffer. Initially, the use of tris-NaCl buffer in the channel led to the formation of air bubbles on the surfaces of both the cathode and anode. As these air bubbles moved upward to escape, they created turbulence and disrupted the buffer flow within the channel, as well as inducing current irregularities in electrophoresis. To address this issue, tris-glycine buffer was introduced as an alternative, effectively preventing the formation of air bubbles and ensuring stable current for electrophoresis.

The channel of GSFE, shown in Fig. 1, was filled with tris-glycine buffer before sample loading and applying the voltage. As illustrated in Fig. 1, Upon injection of GO suspension into the channel, GO nanosheets are subjected to three primary forces: (1) the electric force (F_{el}) generated by the applied voltage through the electrodes, (2) the gravitational force (F_g) due to the mass of the nanosheets, and (3) the frictional force arising from the interaction of the GO nanosheets with the channel walls as well as the frictions between the GO nanosheets and the buffer molecules that GO are suspended (referred to as the friction wall). GO nanosheets, while moving inside the channel, experience both fluid friction and wall interactions. The fluid friction, governed by Stokes' law, arises from contact of GO nanosheets with solvent molecules and opposes both electrophoretic and gravitational motions. Simultaneously, GO nanosheets interact with channel walls through van der Waals forces, electrostatic interactions, and surface roughness effects. While macroscopic friction typically describes solid-solid contact, at micro/nanoscales, friction emerges from the complex interplay of these surface forces and differs fundamentally from classical behavior. When these interactions are high enough that electrical and/or gravitational forces are not adequate to overcome it, then adsorption happens. This distinction is particularly important for 2D materials like GO, where high surface area increase wall interactions [48–50]. The separation channel is inclined at an angle θ, which plays a critical role in the separation process. If θ = 90°, the GO nanosheets rapidly descend the channel without sufficient time for size-based separation. Conversely, at very low values of θ, the nanosheets tend to deposit on the friction wall, either remaining stationary or moving at such a slow rate that they are predominantly influenced by the F_{el}. Only this results in high deflection angles (α) and causes the nanosheets to enter the anode electrode chamber rather than being collected in the designated glass vials. Under optimized conditions, the GO nanosheets are effectively separated based on their sizes due to the interplay of the three forces: electric, gravitational, and frictional forces. The nanosheets are deflected at an angle α, which is determined by the balance of these forces, and are subsequently collected in glass vials. Importantly, this method is not limited to the specific GO nanosheets used in this study. By adjusting the parameters (e.g., electric field strength, channel angle, and buffer composition), the GSFE technique can be applied to separate other GO nanosheets with varying sizes and oxidation degrees. The fundamental principle of size-dependent separation driven by the balance of F_{el}, F_g, and frictional forces ensures the broad applicability of this approach to a wide range of GO samples.

In a colloidal suspension, the settlement of GO nanosheets depends on a several parameters including but not limited to size, mass, charge, and shape of nanosheets.

The theoretical calculation considers Stokes' law (Eq. (1)) which is well developed for spherical particles.

$$v = \left(\frac{2}{9}\right)\frac{(\rho_p - \rho_f)\, gr^2}{\eta} \quad (1)$$

where v denotes the terminal velocity of a spherical particle settling in a viscous fluid, ρ_p represents the particle density, ρ_f the fluid density, g the gravitational acceleration (9.81 m/s^2), r the particle radius, and η the fluid viscosity [51]. Considering the shape of GO this calculation deviates from experimental observations, but provides a general conclusion that mass of $>10^{-22}$ g and size greater than 50 nm will cause settling by gravity. This is in line with observation that vial F1 shows the size distribution of 75 nm.

The minimum voltage to have an acceptable resolution in electrophoresis, the second dimension of GSFE, is in the V range based on the limitation on power supply that was used for the setup. This imposes a practical limitation on the setup that was used for GSFE.

Furthermore, previous studies have demonstrated that similar approaches can be effectively applied to a wide range of GO samples. For example, successfully separated GO sheets with different oxidation levels and sizes using analogous methods [52–54]. Based on these findings and the fundamental principles of this technique, GSFE can be extended to other GO samples.

2.5. Capillary electrophoresis analysis

The fractions collected from the GSFE separation channels were further evaluated using an Agilent G1600AX capillary electrophoresis system. A capillary column with an inner diameter (ID) of 50 μm and outer diameter (OD) of 360 μm with 48.5 cm total long, and 40 cm lengths to the detection window was used for electrophoresis. Tris base-NaCl buffer (pH 10.5) served as the background electrolyte and a voltage of 15 kV (resulting in 68 μA current) with positive polarity was applied for electrophoretic separation of each fractions. The injection was performed by applying 50 mbar pressure for 15 s. Column conditioning involved flushing with 0.1 mol l^{-1} NaOH for 10 min, followed by deionized water for 10 min. The buffer was then flushed through the column for 8 min, with a 10 min buffer flush between runs. The temperature of the cassette was set at 24 ° C, and the run time was set to 10 min. Additionally, the detector was configured to record three wavelengths: 200, 273, and 337 nm and the response time of detector was 0.1 s.

2.6. Characterization of GO fractions

The GSFE fractions were collected for further characterization. The UV–Vis spectrophotometer (Photonix, Iran) was used to record the spectra in the range of 190 to 800 nm. The electropherograms of the fractions were obtained using a G1600AX (Agilent, Germany) capillary electrophoresis instrument. For each collected fraction, the zeta potential measurements were performed using a Zeta compact (CAD, France). The Transmission Electron Microscopy (TEM) analysis of the fractions was performed using a Leo 912AB (ZEISS, Germany) instrument.

2.7. Buffer compatibility

The collected fractions should undergo different tests under specific conditions, and GO must be dispersed in an appropriate solvent for that particular characterization. For instance, to test zeta potential, GO was dispersed in tris-glycine buffer. For capillary electrophoresis experiment and TEM imaging, GO was dispersed in tris base-NaCl buffer and water, respectively. However, this process of changing the buffer to an appropriate one may lead to the loss of small particles due to washing and centrifugation. However, in the GSFE technique, changing the buffer, in which GO should be dispersed for a specific experiment, is straightforward.

Separation by GSFE and by CE may require two different buffers for optimized performance of each technique. For GSFE separation, the optimized buffer was chosen as tris-glycine buffer, whereas for CE the best resolution was obtained in tris-NaCl buffer, pH 10.5. Changing the buffer from tris-glycine to tris-NaCl requires the complete removal of initial buffer, and suspending GO sheets in tris-NaCl for CE analysis. This step is time consuming and will cause the loss of GO nanosheets. Therefore, GO nanosheets were collected directly in tris-NaCl buffer to avoid the change of buffer. During this process, a minute amount of tris-glycine (1.3 μl) will enter into the collecting vials containing 1 ml of tris-NaCl. This will cause no significant change in CE buffer capacity (about 0.13 percent dilution).

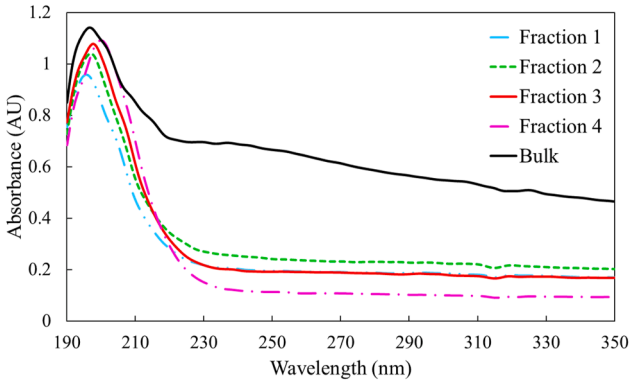

Fig. 2. UV–Vis absorption spectra (190–350 nm) of GO bulk and collected fractions after 1:5 dilution with deionized water. A deionized water blank used for background subtraction.

3. Results and discussion

3.1. Optical properties

A UV–Vis spectrophotometer (190 to 350 nm) was used to investigate the optical properties of bulk GO and each collected fraction. The results are depicted in Fig. 2.

In GO nanosheets, λ_{max} changes with particle size due to factors such as quantum effects, surface effects, and light scattering. These factors cause the optical properties of nanoparticles to change, resulting in different λ_{max} values for each fraction.

When particle size decreases, quantum effects can affect the electronic structure and thus the optical properties of the material. For small nanoparticles, the energy gap between electron levels is described by Eq. (2) [55].

$$E_g = E_{g_{(\infty)}} + \frac{C}{r^2} \quad (2)$$

In this equation E_g, $E_{g_{(\infty)}}$, r and C are the energy gap for a nanoparticle of size r, energy gap in the bulk state, the radius of the nanoparticle and a proportionality constant that depends on the properties of the material, respectively. For non-circular and for non-spherical GO nanosheets, the r can be estimated through various methods including dynamic light scattering, atomic force microscopy, or TEM. In this study, the nanosheet dimensions was quantified via TEM (see Section 3.4 for details), which provides direct measurements of lateral sizes.

Smaller nanoparticles have a higher surface-to-volume ratio, and show dominant surface effects. These surface effects can significantly influence the optical properties of nanoparticles, as the presence of oxygen-containing functional groups (such as carboxyl and hydroxyl group) on their surfaces plays a critical role in modifying their behavior. The interaction of these functional groups with light or other external stimuli such as Au atoms can lead to changes in absorption, scattering, or emission characteristics, thereby impacting the overall optical performance of the nanoparticles [56,57]. As the surface-to-volume ratio

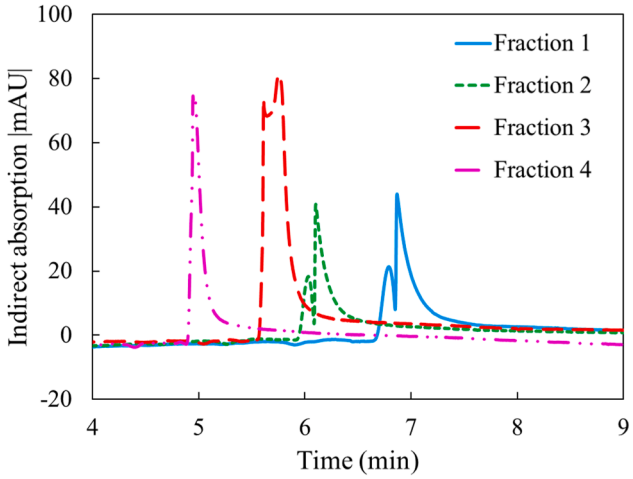

Fig. 3. Electropherograms of collected fractions using UV detection at 200 nm. F1, F2. F3 and F4 (from smallest to biggest) are the fractions 1, 2, 3 and 4 collected from vials shown in Fig. 1. A 50 μm ID capillary (48.5 cm total length, 40 cm to detector) was used. The background electrolyte was tris-NaCl buffer (50 mmol l^{-1} tris, 93 mmol l^{-1} NaCl, pH 10.5). Separation was performed at 15 kV and 68 μA with positive polarity. Samples were injected at 50 mbar for 15 s. The column was conditioned with 0.1 M NaOH (10 min), DI water (10 min), and buffer (8 min pre-run, 10 min between runs). The cassette temperature was maintained at 24 °C, and runs lasted for 10 min. Detection was performed at 200 nm with a 0.1 s detector response time. Detection was performed using indirect absorption. The absolute value of absorption |mAu| is shown in Y axis for visual purpose.

increases in smaller particles, the number density of surface functional groups increases. These functional groups lead to the formation of chemical bonds and the creation of more areas with high surface charge density, which shifts the absorption wavelength to shorter wavelengths (Blue shift). Consequently, F1 fraction has the lowest λ_{max} (195.4 nm), while F4 fraction has the highest λ_{max} (200.7 nm) value.

To calculate the energy gap (E_g) from the λ_{max} for each fraction, the Planck relation (Eq. (3)) might be used.

$$E_g = \frac{hc}{\lambda} \tag{3}$$

In this equation h, c, and λ are Planck's constant (6.626×10^{-34} J s), the speed of light (3×108 m per second) and the wavelength (in meters), respectively.

The energy gap for each fraction was calculated using Eq. (3), and the values for F1 and F4 are 1.02×10^{-18} and 0.98×10^{-18}J, respectively. From Eqs. (2) and (3), it can be concluded that decreasing the size of the particles will cause an increase in the energy gap and the maximum wavelength will shift to lower wavelengths. By decreasing size of each collected fraction, a distend blue shift was observed (see Fig. 2). This result has been confirmed elsewhere [52]. Based on literatures, red shift might be due to longer drying time and, therefore, coagulation of nanoparticles. The blue shift observation by decreasing in size confirms both the efficiency of preparing nanoparticles, as well as the quantum conferment effect [58].

3.2. Results of capillary electrophoresis

Capillary electrophoresis (CE) is a powerful and high-resolution technique for size-based separation of nanomaterials and biomaterials [40,59–63]. However, its main limitation lies in the small amount of sample loading and the minute fractions collected after each separation. Under counter-EOF conditions (where |μEOF| > |μep|), the apparent mobility is calculated as the difference between the absolute values of EOF mobility and effective electrophoretic mobility.

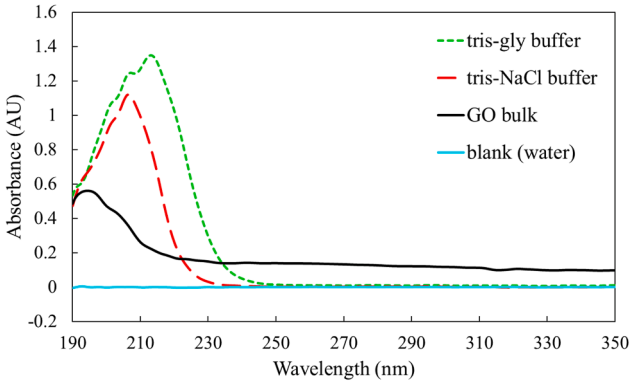

Fig. 4. UV–Vis absorption spectra (190–350 nm) of bulk GO (diluted 1:5 with deionized water), tris-NaCl buffer (50 mmol l^{-1} tris), and tris-gly buffer (20 mmol l^{-1} tris and 20 mmol l^{-1} glycine), using deionized water as the blank.

$$|\mu_{app}| = |\mu_{EOF}| - |\mu_{ep}| \tag{4}$$

where μ_{app}, μ_{ep} and μ_{eo} are apparent mobility, electrophoretic mobility and electroosmotic mobility, respectively. The CE instrument settings were configured as described in Section 2.4. In positive polarity, anode is the positive electrode, while the cathode is negative. Applying a voltage creates an electroosmotic flow. Typically, the electroosmotic flow exceeds the electrophoretic mobility, resulting in the movement of all particles towards the cathode. Considering the positive polarity of the device and the greater mobility of smaller particles, the migration times of smaller particles will be longer.

DMSO was used as the neutral marker. The migration time of DMSO was 4.4 min. That was used to calculate electroosmotic flow (EOF) mobility. As it could be observed in Fig. 3, Fraction 1 which contains the smallest nanosheets, has the highest effective electrophoretic mobility and lowest apparent electrophoretic mobility and longest migration time when compared to those of other fractions.

As shown in Fig. 3, the peaks associated with fractions 1, 2, and 3 exhibit splitting, indicating that the GO nanosheets within each fraction are not completely uniform in size and the resolution of GSFE is not ideal, and span a range of dimensions. To achieve greater size uniformity, these fractions can be further separated into sub-fractions with narrower size ranges using capillary electrophoresis. By optimizing the experimental conditions of capillary electrophoresis, each fraction obtained from GSFE can be subdivided into multiple fractions, resulting in a more precise size distribution of the GO nanosheets.

Before running the CE experiments, in order to choose the best wavelength for DAD, the UV–Vis absorbance of the tris-NaCl buffer (50 mmol l^{-1} tris), tris-gly buffer (20 mmol l^{-1} tris and 20 mmol l^{-1} glycine), and diluted suspension of the bulk GO (at a 1:5 ratio with deionized water) was recorded using a spectrophotometer, with deionized water as the blank. The results are presented in Fig. 4. As shown in this figure, the absorbance of GO at 200 nm is lower than that of the tris-NaCl buffer used as run buffer in the CE experiment. As a result, automatic background correction of the peaks obtained during the CE analysis subtracts the absorbance of tris-NaCl from that of GO suspension in deionized water, injected as a plug on the CE column, that are collected from the vials of GSFE. This will result in negative peaks. By switching the Agilent ChemStation software to an indirect UV detection mode, these peaks was recorded positive.

3.3. Zeta potential

The Smoluchowski equation (Eq. (5)) is one of the key equations for calculating the electrophoretic mobility (μ_{ep}) in colloidal systems, relating the zeta potential (ζ) to (μ_{ep}).

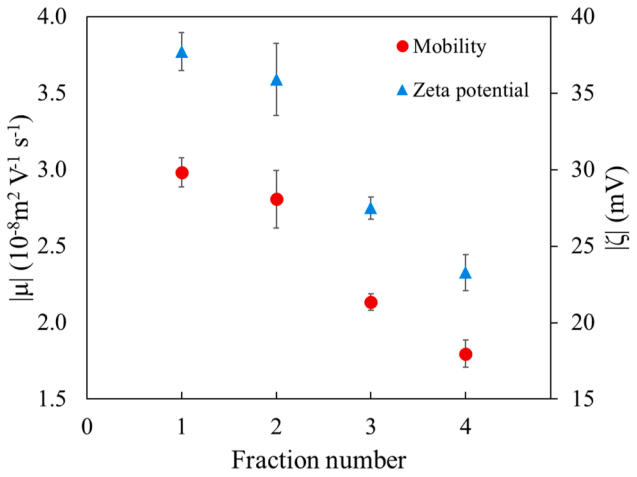

Fig. 5. Zeta potential and electrophoretic mobility of collected fractions.

$$\mu = \frac{\varepsilon_r \varepsilon_0 \zeta}{\eta} \tag{5}$$

where ζ, η, ε_r and ε_0 are zeta potential (in V or mV), electrophoretic mobility (in $10^{-8}m^2V^{-1}s^{-1}$), viscosity of the medium (in Pa.s), the solution relative permittivity and the permittivity of the vacuum, respectively [64].

The electrophoretic mobility depends on the surface charge of the particle and the distribution of ions around it. For particles of different sizes, zeta potential changes, which in turn alters the electrophoretic mobility. Therefore, if r (particle radius) decreases while the ionic strength medium remains constant, zeta potential increases.

Fig. 5 demonstrates the changes in zeta potential and mobility with variations in particle size. As the particles become smaller, the number of functional groups on the surface and edges of the GO nanosheets increases in proportion to the surface area. As a result, the zeta potential and mobility also increase.

The results obtained from the zeta potential test cross validates the findings from UV–Vis spectroscopy and capillary electrophoresis. These results also indicate the separation of particles based on size in the GSFE technique.

3.4. Morphology of fractions

To confirm the results of zeta potential, optical spectroscopy, and capillary electrophoresis, the morphology and the average particle size of collected fractions were examined by recording TEM image for fractions 1, 4 and bulk (Fig. 6). The TEM image of fraction 1 shows the graphene oxide particles with the smallest size among the examined fractions. The particles in this image are very small and well-dispersed, indicating the success of separating small particles. The average particle size in this fraction was about 75 nm.

Fraction 4 contains the largest GO nanosheets among the four collected fractions. The TEM image shows large and less dispersed particles compared to other fractions. The TEM images validate the experiments on particle size separation. The size distribution of the particles in this fraction is around 450 nm. This image confirms that the larger particles are also well separated. Finally, the results of the analysis of TEM images show the success of the separation process of graphene oxide particles based on size. Fraction 1 contained the smallest particles, and Fraction 4 contained the largest particles. The bulk was also used as a reference for comparison and showed a wider distribution of particle sizes.

4. Conclusions

The GSFE technique is presented here, for the first time, as a novel approach for size-based fractionation of graphene oxide. The results demonstrated that this technique has a high separation ability without

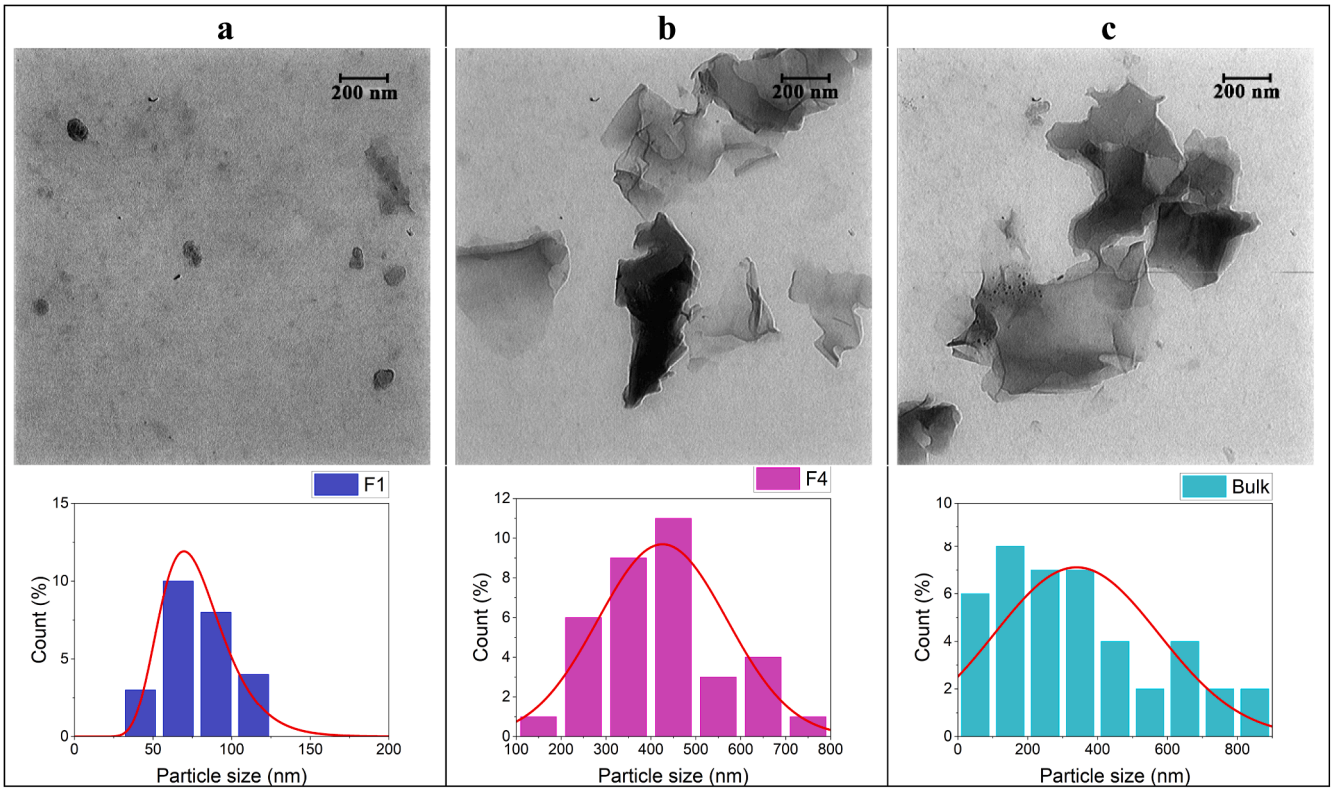

Fig. 6. The TEM image of Fractions 1,4 and bulk of GO and their histograms (a, b and c respectively).

the limitations and issues of classical techniques. The advantages of this new technique include automation capability, high-throughput fractionation, scalability, good resolution, high speed, continues separation and low cost.

The GSFE technique introduced here, addresses a large part of the limitations in preparative capillary electrophoresis. Characterization methods applied to each collected fractions were well correlated with the size of each fraction and their corresponding properties. The UV–Vis spectroscopy (Stokes shift from 195.4 nm to 200.7 nm), capillary electrophoresis (migration time between 5 min to 6.8 min), zeta potential (23.3 mV for the largest particle changed to 37.7 mV for the smallest particle), mobility (2.9×10^{-8} $m^2V^{-1}s^{-1}$ for the smallest particle changed to 1.8×10^{-8} $m^2V^{-1}s^{-1}$ for the largest particle), and TEM for each fraction showed distinct differences among the bulk and each fraction. The effective radius (r) of GO nanosheets was determined directly from TEM measurements, eliminating the need for spherical approximations. For fraction 1 (smallest nanosheets), the average radius was ~37 nm, whereas fraction 4 (largest nanosheets) exhibited an average radius of ~225 nm.

Given their anisotropic shape and surface charge effects, the actual sedimentation behavior of these 2D nanosheets may deviate significantly from spherical model predictions. Nevertheless, the TEM-derived dimensions represent the most accurate empirical basis for analysis. Furthermore, the results demonstrated that this technique has a high separation power without some of the limitations of classical separation methods. Finally, the most important limitation of capillary electrophoresis was resolved by significantly improving the throughput of separation.

CRediT authorship contribution statement

Masoud Shayegan: Writing – original draft, Software, Methodology, Investigation, Funding acquisition, Formal analysis, Data curation. **Hossein Ahmadzadeh:** Writing – review & editing, Validation, Supervision, Project administration, Conceptualization.

Declaration of competing interest

The authors declare no conflict of interests.

Acknowledgements

The authors thank Ferdowsi University of Mashhad (FUM) for supporting this project (3/61039).

Data availability

Data will be made available on request.

References

[1] B. Bhushan, Introduction to nanotechnology, in: B. Bhushan (Ed.), Springer Handbook of Nanotechnology, Springer Berlin Heidelberg, Berlin, Heidelberg, 2017, pp. 1–19, https://doi.org/10.1007/978-3-662-54357-3_1.
[2] N. Joudeh, D. Linke, Nanoparticle classification, physicochemical properties, characterization, and applications: a comprehensive review for biologists, J. Nanobiotechnology. 20 (1) (2022) 262, https://doi.org/10.1186/s12951-022-01477-8.
[3] N. Tabassum, Z.N. Georgieva, G.H. Debnath, D.H. Waldeck, Size-dependent chiro-optical properties of CsPbBr3 nanoparticles, Nanoscale 15 (5) (2023) 2143–2151, https://doi.org/10.1039/D2NR06751J.
[4] X. Li, X. Tong, Q. Chen, H. Liu, Size effect of graphene oxide sheets on enantioseparation performances in membrane separation, Colloid. Surfaces A 618 (2021) 126464, https://doi.org/10.1016/j.colsurfa.2021.126464.
[5] W. Gao, The chemistry of graphene oxide, in: W. Gao (Ed.), Graphene Oxide: Reduction Recipes, Spectroscopy, and Applications, Springer International Publishing, Cham, 2015, pp. 61–95, https://doi.org/10.1007/978-3-319-15500-5_3.
[6] S. Eissa, J. N'diaye, P. Brisebois, R. Izquierdo, A.C. Tavares, M. Siaj, Probing the influence of graphene oxide sheets size on the performance of label-free electrochemical biosensors, Sci. Rep. 10 (1) (2020) 13612, https://doi.org/10.1038/s41598-020-70384-5.
[7] K.Z. Donato, H.L. Tan, V.S. Marangoni, M.V.S. Martins, P.R. Ng, M.C.F. Costa, P. Jain, S.J. Lee, G.K.W. Koon, R.K. Donato, A.H. Castro Neto, Graphene oxide classification and standardization, Sci. Rep. 13 (1) (2023) 6064, https://doi.org/10.1038/s41598-023-33350-5.
[8] L. An, D. Zhang, L. Zhang, G. Feng, Effect of nanoparticle size on the mechanical properties of nanoparticle assemblies, Nanoscale 11 (19) (2019) 9563–9573, https://doi.org/10.1039/C9NR01082C.
[9] H. Zhang, H. Zhu, C. Xu, Y. Li, Q. Liu, S. Wang, S. Yan, Effect of nanoparticle size on the mechanical properties of polymer nanocomposites, Polymer. (Guildf) 252 (2022) 124944, https://doi.org/10.1016/j.polymer.2022.124944.
[10] J. Kim, S.W. Kim, H. Yun, B.J. Kim, Impact of size control of graphene oxide nanosheets for enhancing electrical and mechanical properties of carbon nanotube–polymer composites, RSC. Adv. 7 (48) (2017) 30221–30228, https://doi.org/10.1039/C7RA04015F.
[11] M. Davardoostmanesh, H. Ahmadzadeh, E.K. Goharshadi, A. Meshkini, E. Sistanipour, Electrophoretic extraction of highly monodispersed graphene quantum dots from widely polydispersed bulk and its cytotoxicity effect against cancer cells, Microchem. J. 159 (2020) 105391, https://doi.org/10.1016/j.microc.2020.105391.
[12] A. Gautam, P. Komal, P. Gautam, A. Sharma, N. Kumar, J.P. Jung, Recent trends in noble metal nanoparticles for colorimetric chemical sensing and micro-electronic packaging applications, Metals. (Basel) 11 (2) (2021) 329, https://doi.org/10.3390/met11020329.
[13] F. Foroutan, H. Ahmadzadeh, M. Davardoostmanesh, A. Amiri, Water desalination using stainless steel meshes coated with layered double hydroxide/graphene oxide nanocomposite, Water Environ. Res. 95 (9) (2023) 10925, https://doi.org/10.1002/wer.10925.
[14] Z. Han, L. Sun, Y. Chu, J. Wang, C. Wei, Y. Liu, Q. Jiang, C. Han, H. Yan, X. Song, Ultrasonication-tailored graphene oxide of varying sizes in multiple-equilibrium-route-enhanced adsorption for aqueous removal of acridine orange, Molecules. 28 (10) (2023) 4179, https://doi.org/10.3390/molecules28104179.
[15] M. Liu, Y. Wang, Y. Wu, C. Liu, X. Liu, Preparation of graphene oxide hydrogels and their adsorption applications toward various heavy metal ions in aqueous Media, Appl. Sci. 13 (21) (2023) 11948, https://doi.org/10.3390/app132111948.
[16] S.M. Mousavi, S.A. Hashemi, M.Y. Kalashgrani, A. Gholami, M. Binazadeh, W.-H. Chiang, M.M. Rahman, Recent advances in energy storage with graphene oxide for supercapacitor technology, Sustain. Energy Fuels. 7 (21) (2023) 5176–5197, https://doi.org/10.1039/D3SE00867C.
[17] M.A. Ashraf, W. Peng, Y. Zare, K.Y. Rhee, Effects of size and aggregation/agglomeration of nanoparticles on the interfacial/interphase properties and tensile strength of polymer nanocomposites, Nanoscale Res. Lett. 13 (1) (2018) 214, https://doi.org/10.1186/s11671-018-2624-0.
[18] C. Caizer, Nanoparticle size effect on some magnetic properties, in: M. Aliofkhazraei (Ed.), Handbook of Nanoparticles, Springer International Publishing, Cham, 2016, pp. 475–519, https://doi.org/10.1007/978-3-319-15338-4_24.
[19] V.A. Eremeyev, Size effect in nanomaterials, in: H. Altenbach, A. Öchsner (Eds.), Encyclopedia of Continuum Mechanics, Springer Berlin Heidelberg, Berlin, Heidelberg, 2020, pp. 2290–2291, https://doi.org/10.1007/978-3-662-55771-6_170.
[20] Y. Su, Current State-of-the-art membrane based filtration and separation technologies, in: H. Zhu, P. Sun (Eds.), Graphene-based Membranes for Mass Transport Applications, The Royal Society of Chemistry, 2018, pp. 1–13, https://doi.org/10.1039/9781788013017-00001.
[21] J.D. Robertson, L. Rizzello, M. Avila-Olias, J. Gaitzsch, C. Contini, M.S. Magoń, S. A. Renshaw, G. Battaglia, Purification of nanoparticles by size and shape, Sci. Rep. 6 (1) (2016) 27494, https://doi.org/10.1038/srep27494.
[22] H. Guo, G. Stan, Y. Liu, Nanoparticle separation based on size-dependent aggregation of nanoparticles due to the critical Casimir effect, Soft. Matter. 14 (8) (2018) 1311–1318, https://doi.org/10.1039/C7SM01971H.
[23] M.A. Ibrahim, M.Z. Jaafar, M.A. Md Yusof, A.K. Idris, A review on the effect of nanoparticle in drilling fluid on filtration and formation damage, J. Petroleum Sci. Eng. 217 (2022) 110922, https://doi.org/10.1016/j.petrol.2022.110922.
[24] O. Akbulut, C.R. Mace, R.V. Martinez, A.A. Kumar, Z. Nie, M.R. Patton, G. M. Whitesides, Separation of nanoparticles in aqueous multiphase systems through centrifugation, Nano Lett. 12 (8) (2012) 4060–4064, https://doi.org/10.1021/nl301452x.
[25] Y. Asnaashari Kahnouji, E. Mosaddegh, M.A. Bolorizadeh, Detailed analysis of size-separation of silver nanoparticles by density gradient centrifugation method, Mater. Sci. Eng. 103 (2019) 109817, https://doi.org/10.1016/j.msec.2019.109817.
[26] Y. Mori, Size-selective separation techniques for nanoparticles in liquid, KONA Powder Particle J. 32 (2015) 102–114, https://doi.org/10.14356/kona.2015023.
[27] H.J. Choi, M. Ko, I.H. Kim, H. Yu, J.Y. Kim, T. Yun, J.S. Yang, G.G. Yang, H. S. Jeong, M.H. Moon, S.O. Kim, Wide-range size fractionation of graphene oxide by flow field-flow fractionation, ACS. Nano 16 (6) (2022) 9172–9182, https://doi.org/10.1021/acsnano.2c01402.
[28] M. Ko, H.J. Choi, J.Y. Kim, I.H. Kim, S.O. Kim, M.H. Moon, Optimization for size separation of graphene oxide sheets by flow/hyperlayer field-flow fractionation, J. Chromatogr. A 1681 (2022) 463475, https://doi.org/10.1016/j.chroma.2022.463475.
[29] M. Moon, Frit-inlet asymmetrical flow field-flow fractionation (FI-AFlFFF): a stopless separation technique for macromolecules and nanoparticles, Bull. Korean Chem. Soc. 22 (2001) 337–348.

[30] C. Contado, P. Reschiglian, S. Faccini, A. Zattoni, F. Dondi, Continuous split-flow thin cell and gravitational field-flow fractionation of wheat starch particles, J. Chromatogr. A 871 (1) (2000) 449–460, https://doi.org/10.1016/S0021-9673(99)01191-7.
[31] V. Kašička, Z. Prusik, J. Pospíšek, Conversion of capillary zone electrophoresis to free-flow zone electrophoresis using a simple model of their correlation: application to synthetic enkephalin-type peptide analysis and preparation, J. Chromatogr. A 608 (1) (1992) 13–22, https://doi.org/10.1016/0021-9673(92)87101-D.
[32] V. Kašička, Z. Prusík, P. Sázelová, J. Jiráček, T. Barth, Theory of the correlation between capillary and free-flow zone electrophoresis and its use for the conversion of analytical capillary separations to continuous free-flow preparative processes: application to analysis and preparation of fragments of insulin, J. Chromatogr. A 796 (1) (1998) 211–220, https://doi.org/10.1016/S0021-9673(97)01114-X.
[33] V. Kasicka, From micro to macro: conversion of capillary electrophoretic separations of biomolecules and bioparticles to preparative free-flow electrophoresis scale, Electrophoresis 30 (1) (2009) S40–S52, https://doi.org/10.1002/elps.200900156. Suppl.
[34] B. Kowalczyk, I. Lagzi, B.A. Grzybowski, Nanoseparations: strategies for size and/or shape-selective purification of nanoparticles, Curr. Opin. Colloid. Interface Sci. 16 (2) (2011) 135–148, https://doi.org/10.1016/j.cocis.2011.01.004.
[35] A. Olatunde, M.S. Obidola, H. Tijjani, Chapter 3 - centrifugation techniques, in: C. Egbuna, K.C. Patrick-Iwuanyanwu, M.A. Shah, J.C. Ifemeje, A. Rasul (Eds.), Analytical Techniques in Biosciences, Academic Press, 2022, pp. 43–58, https://doi.org/10.1016/B978-0-12-822654-4.00008-7.
[36] J. Liderfelt, J. Royce, Chapter 14 - filtration principles, in: G. Jagschies, E. Lindskog, K. Łącki, P. Galliher (Eds.), Biopharmaceutical Processing, Elsevier, 2018, pp. 279–293, https://doi.org/10.1016/B978-0-08-100623-8.00014-1.
[37] A. Bardhan, A. Akhtar, S. Subbiah, Chapter 1 - microfiltration and ultrafiltration membrane technologies, in: S.K. Nayak, K. Dutta, J.M. Gohil (Eds.), Advancement in Polymer-Based Membranes For Water Remediation, Elsevier, 2022, pp. 3–42, https://doi.org/10.1016/B978-0-323-88514-0.00001-2.
[38] J. Zhao, G. Chen, W. Zhang, P. Li, L. Wang, Q. Yue, H. Wang, R. Dong, X. Yan, J. Liu, High-resolution separation of graphene oxide by capillary electrophoresis, Anal. Chem. 83 (23) (2011) 9100–9106, https://doi.org/10.1021/ac202136n.
[39] C. Adelantado, B.H. Lapizco-Encinas, J. Jordens, S. Voorspoels, M. Velimirovic, K. Tirez, Capillary electrophoresis as a complementary analytical tool for the separation and detection of nanoplastic particles, Anal. Chem. 96 (19) (2024) 7706–7713, https://doi.org/10.1021/acs.analchem.4c00822.
[40] M. Bouri, R. Salghi, M. Algarra, M. Zougagh, A. Ríos, A novel approach to size separation of gold nanoparticles by capillary electrophoresis–evaporative light scattering detection, RSC. Adv. 5 (22) (2015) 16672–16677, https://doi.org/10.1039/C4RA17217E.
[41] J.A. Preuss, G.N. Nguyen, V. Berk, J. Bahnemann, Miniaturized free-flow electrophoresis: production, optimization, and application using 3D printing technology, Electrophoresis 42 (3) (2021) 305–314, https://doi.org/10.1002/elps.202000149.
[42] F. Barbaresco, M. Cocuzza, C.F. Pirri, S.L. Marasso, Application of a micro free-flow electrophoresis 3D printed lab-on-a-chip for micro-nanoparticles analysis, Nanomaterials. (Basel) 10 (7) (2020), https://doi.org/10.3390/nano10071277.
[43] P. Novo, D. Janasek, Current advances and challenges in microfluidic free-flow electrophoresis—A critical review, Anal. Chim. Acta 991 (2017) 9–29, https://doi.org/10.1016/j.aca.2017.08.017.
[44] K. Broeckhoven, G. Desmet, Advances and challenges in extremely high-pressure liquid chromatography in current and future analytical scale column formats, Anal. Chem. 92 (1) (2020) 554–560, https://doi.org/10.1021/acs.analchem.9b04278.
[45] L. Zhang, Z. Li, Y. Zhang, M. Chin Paau, Q. Hu, X. Gong, S. Shuang, C. Dong, X. Peng, M.M.F. Choi, High-performance liquid chromatography coupled with mass spectrometry for analysis of ultrasmall palladium nanoparticles, Talanta 131 (2015) 632–639, https://doi.org/10.1016/j.talanta.2014.08.032.
[46] J. Bian, N. Gobalasingham, A. Purchel, J. Lin, The power of field-flow fractionation in characterization of nanoparticles in drug delivery, Molecules. 28 (10) (2023) 4169.
[47] B. Zhang, S.-X. Zhang, R. Yao, Y.-H. Wu, J.-S. Qiu, Progress and prospects of hydrogen production: opportunities and challenges, J. Electr. Sci. Technol. 19 (2) (2021) 100080, https://doi.org/10.1016/j.jnlest.2021.100080.
[48] Y. Song, E. Meyer, Atomic friction processes of two-dimensional materials, Langmuir. 39 (44) (2023) 15409–15416, https://doi.org/10.1021/acs.langmuir.3c01546.
[49] A.J. Weymouth, O. Gretz, E. Riegel, F.J. Giessibl, Measuring sliding friction at the atomic scale, Jpn. J. Appl. Phys. 61 (SL) (2022) SL0801, https://doi.org/10.35848/1347-4065/ac5e4a.
[50] G. Wu, S. Ogata, L. Gao, Atomistic simulations of the frictional properties of 2D materials: a review, J. Phys. D. Appl. Phys. 57 (29) (2024) 293001, https://doi.org/10.1088/1361-6463/ad365c.
[51] Y.-Z. Zhang, Y. Wang, T. Cheng, L.-Q. Yao, X. Li, W.-Y. Lai, W. Huang, Printed supercapacitors: materials, printing and applications, Chem. Soc. Rev. 48 (12) (2019) 3229–3264, https://doi.org/10.1039/C7CS00819H.
[52] D.-W. Kang, H.-S. Shin, Control of size and physical properties of graphene oxide by changing the oxidation temperature, Carbon Letters 13 (1) (2012) 39–43, https://doi.org/10.5714/cl.2012.13.1.039.
[53] Z. Benzait, L. Trabzon, Graphite size effect on chemical expansion and graphene oxide properties, ACS. Omega 7 (42) (2022) 37885–37895, https://doi.org/10.1021/acsomega.2c05059.
[54] R.S. Zambare, K.B. Dhopte, P.R. Nemade, C.Y. Tang, Effect of oxidation degree of GO nanosheets on microstructure and performance of polysulfone-GO mixed matrix membranes, Sep. Purif. Technol. 244 (2020) 116865, https://doi.org/10.1016/j.seppur.2020.116865.
[55] G. Cao, Y. Wang, Nanostructures and Nanomaterials: Synthesis, Properties, and Applications, 2 ed., World Scientific, 2011 https://doi.org/10.1142/7885.
[56] D.O. Idisi, E.M. Benecha, Electronic, magnetic, and optical properties of graphene oxide nanosheets doped with Au atoms: a density functional theory study, Europ. Phys. J. Plus 137 (7) (2022) 820, https://doi.org/10.1140/epjp/s13360-022-03046-2.
[57] J. Chen, X. Zhang, X. Zheng, C. Liu, X. Cui, W. Zheng, Size distribution-controlled preparation of graphene oxide nanosheets with different C/O ratios, Mater. Chem. Phys. 139 (1) (2013) 8–11, https://doi.org/10.1016/j.matchemphys.2012.12.025.
[58] A.J. Deotale, R.V. Nandedkar, Correlation between particle size, strain and band gap of iron oxide nanoparticles, Mater. Today 3 (6) (2016) 2069–2076, https://doi.org/10.1016/j.matpr.2016.04.110.
[59] A.J. Chetwynd, E.J. Guggenheim, S.M. Briffa, J.A. Thorn, I. Lynch, E. Valsami-Jones, Current application of capillary electrophoresis in nanomaterial characterisation and its potential to characterise the protein and small molecule corona, Nanomaterials. (Basel) 8 (2) (2018), https://doi.org/10.3390/nano8020099.
[60] S.P. Hartono, H. Ahmadzadeh, Analysis of mitochondrial distribution within muscle fibers as an age dependent factor using direct histological sampling interfaced with capillary electrophoresis with laser-induced fluorescence detector, Abstracts of Papers of The American Chemical Society, Am. Chem. Soc. (2007).
[61] R.D. Johnson, M. Navratil, B.G. Poe, G. Xiong, K.J. Olson, H. Ahmadzadeh, D. Andreyev, C.F. Duffy, E.A. Arriaga, Analysis of mitochondria isolated from single cells, Anal. Bioanal. Chem. 387 (1) (2007) 107–118, https://doi.org/10.1007/s00216-006-0689-6.
[62] C. Adelantado, N. Rodríguez-Fariñas, R.C. Rodríguez Martín-Doimeadios, M. Zougagh, Á. Ríos, Analysis of silica nanoparticles by capillary electrophoresis coupled to an evaporative light scattering detector, Anal. Chim. Acta 923 (2016) 82–88, https://doi.org/10.1016/j.aca.2016.03.055.
[63] C. Adelantado, Á. Ríos, M. Zougagh, A new nanometrological strategy for titanium dioxide nanoparticles screening and confirmation in personal care products by CE-spICP-MS, Talanta 219 (2020) 121385, https://doi.org/10.1016/j.talanta.2020.121385.
[64] S. Štěpánová, V. Kašička, Determination of physicochemical parameters of (bio) molecules and (bio)particles by capillary electromigration methods, J. Sep. Sci. 47 (11) (2024) e2400174, https://doi.org/10.1002/jssc.202400174.